# Influence of the texturing quality consecutive to Abrasive Water Jet machining on the adhesive properties in mode I of 3D woven composite assemblies

X. Sourd, Redouane Zitoune, Laurent Crouzeix, M. Coulaud

Version of Record: https://www.sciencedirect.com/science/article/pii/S135983682200467X
Manuscript_4903c0e2062f79f85bda3e51492b4442

# Influence of the texturing quality consecutive to Abrasive Water Jet machining on the adhesive properties in mode I of 3D woven composite assemblies

X. Sourd[a,b,*], R. Zitoune[a,**], L. Crouzeix[a], M. Coulaud[b]

[a] Institut Clément Ader, CNRS UMR 5312. 3 Rue Caroline Aigle. 31400, Toulouse, France.

[b] Safran Aircraft Engines, Villaroche. Rond-point René Ravaud. 77550, Moissy-Cramayel, France

[*]xavier.sourd@iut-tlse3.fr

[**]redouane.zitoune@iut-tlse3.fr

**Abstract**

The aim of this study is to analyse the suitability of Abrasive Water Jet Machining (AWJM) as a surface preparation technique for adhesive bonding of 3D woven CFRP substrates and to investigate the influence of the texture-induced quality of the adherends on the adhesive properties of the bonded joints. For this, three specimens with varying levels of texturing qualities were produced by AWJM and quantified using classical criteria such as average roughness “Ra and Sa” as well as a new criterion named “crater volume” (Cv). After adhesive bonding, the assemblies with different levels of texturing quality were subjected to Double Cantilever Beam tests to obtain their critical energy release rate in mode I ($G_{Ic}$), which was compared to values of bonded assemblies prepared by sanding as performed in the industrial context. For the analysis of the damage mechanisms, DCB tests were multi-instrumented with different techniques such as X-ray tomography and digital image correlation. The obtained results showed that, the evolution of $G_{Ic}$ as a function of the textured surface quality presented a good correlation with Cv compared to the classical parameter Ra or Sa. In addition, assemblies prepared by AWJM present higher values of $G_{Ic}$ compared to sanded ones (up to +60%), with a downward parabolic relationship between $G_{Ic}$ and Cv. Post-mortem X-Ray tomography analysis has revealed a change in the crack propagation scenario as Cv increases.

Keywords: A - Polymer-matrix composites (PMCs); D - Mechanical testing; D - Surface analysis; E - Machining

# I. Introduction

Due to its specific attributes such as high strength-to-weight ratio and resistance to corrosion, Carbon Fibre Reinforced Polymer (CFRP) composite materials are extensively used in the aerospace field. In this context, three-dimensional interlock woven CFRP has been designed. As they can replace and/or be assembled with metallic materials in structural inner and outer parts, they are prone to damage. In fact, during their service life, these structures face several kind of damage such as impact or erosion. The presence of damage is threat to the aircraft's integrity and its passengers' life. Hence, very strict regulations have been established concerning maintenance by government agencies like the European Aviation Safety Agency (EASA) or the Civil Aviation Authority (CAA). As the aircraft is grounded during the repair operations, leading to rise in overhead costs to the aviation companies, the repair procedure has to be agile while maintaining the mechanical properties of the repaired area close to the undamaged structure. It is important to mention that, in the industrial field, the repair procedure is organized into six phases: (i) damage localization and characterization, (ii) removal of the impaired area, (iii) surface preparation, (iv) patch design, (v) adhesive bonding and finally (vi) inspection and certification. In general, the second step of the repair procedure is performed by conventional machining. However, machining CFRP by conventional process has proven to be unsuitable due to the generation of mechanical and thermal damage which affect the mechanical performances of the machined parts [1–3]. In addition, the complex mechanisms of cutting leadsd to the formation of chips in the form of fine particles which are noxious for the operators [1,4,5]. In fact, based on the work of Nguyen-Dinh et al. [5], for any condition of cutting used, edge trimming of CFRP by conventional process of machining generates particles whose size is inferior to 0.25 µm. Indeed, Abrasive Water Jet (AWJ) process has proven to be a suitable alternative technique to perform such repair operations. Indeed, both heat generation and volatile particles of carbon fibres are neutralized by the water flow [6,7]. Moreover, in the context of repair application by adhesive bonding, Sourd et al. [8] have shown that very low surface contamination by abrasive embedment in 3D woven composite consecutive to AWJ machining can be obtained with the proper selection of process parameters (less than 0,5% of the milled surface). In addition, a wise choice of machining parameters (viz. jet pressure, traverse speed, etc.) leads to obtain both the target depth of removal and the desired surface quality [8–11]. Several authors have proposed prediction models of depth of removal [9] and surface roughness [12,13] consecutive to AWJ machining in CFRP. It is clearly mentioned that the predicted values of depth and roughness given by these models

are in close agreement with the experimental results, with all the mean errors under 5%. Given that the quality of textured surface of the adherends is a key parameter for a performant adhesive bond, it might be interesting to consider the AWJ process as a surface preparation of the substrates.

Indeed, surface preparation is essential to promote and/or strengthen the adhesive bond, mainly by mechanical or chemical alteration of the adherent's surface, leading to an increase in the surface roughness. The adhesive then fills the irregularities generated by roughening, which enhances the intermolecular bonds and interlocking of the adherents [14,15]. A non-linear relationship between the average roughness Ra of the aluminum substrate and the fracture resistance of the epoxy–aluminium interface was found by Zhang et al. [16] thanks to Double Cantilever Beam (DCB) tests. This non-linearity, explained by bridging and friction behind the crack, shows that the fracture of the interface is piloted by a wider scale surface quality indicator than the nanoscale features observed on the aluminium surface. Hejjaji et al. [17] performed removal of plies from CFRP laminates made of unidirectional plies by AWJ milling process and studied the influence of induced surface quality on the tensile behaviour of patched plies adhesion replicating repair operation. The authors concluded that the tensile strength of the bonded assemblies varied with the damage level of the milled adherents. However, these changes are not significant enough to directly link the surface quality of the adherent and the adhesive properties of the assemblies. It is then suggested to perform DBC tests and shear tests on single lap specimens to further analyse this relationship. Though several studies investigate the adhesive properties in mode I of CFRP/CFRP assemblies made of 3D woven CFRP composite adherents [18–21], to the authors knowledge, no study has been yet performed on the relationship between the surface quality induced by AWJ texturing of the adherents and the adhesive properties of the assemblies.

The aim of this study is then to investigate the link between the surface quality induced by AWJ texturing of 3D woven CFRP adherents and the mechanical performances of the CFRP/CFRP bonded assemblies. In this context, specimens have been textured by Abrasive Water Jet process with three surface qualities, using different levels of jet pressure, traverse speed of the machining head as well as standoff distance and scan step. The obtained surfaces are then characterized in order to quantify the amount of damage generated by AWJ texturing operation thanks to profilometry to measure the crater volume (Cv), the average surface roughness (Ra) and the arithmetical mean height (Sa) surface parameters. The specimens with similar surface qualities are then bonded using an epoxy adhesive film. The bond of the assemblies is inspected by X-ray tomography analysis and Double Cantilever Beam

(DCB) tests are performed. For the damage analysis, DCB tests have been multi-instrumented by a Digital Image Correlation (DIC) device to analyse the strain distributions and to follow the crack propagation as well as X-ray tomography for the observation of the crack propagation path. The assemblies are finally subjected to post-mortem analysis using X-ray tomography test to investigate the crack propagation and damage mechanisms occurring during the tests. All these results permit to correlate the textured surface quality (Cv) and the critical energy release rate in mode I of the bonded assemblies, in addition to link it to the changes in crack propagation mechanisms.

# II. Material and methods

## II.1. Material

In this study, a plate made of CFRP 3D woven composite has been manufactured by light Resin Transfer Moulding. This 4.7 mm thick plate is constituted of IM7 (Hexcel Composites Company) carbon fibres and PR520 (Cytec Company) epoxy resin and has a nominal fibre volume fraction of around 54%. Further details (e.g. weaving architecture, mechanical properties, etc…) of this material might be provided based on request and approval from Safran Aircraft Engines.

## II.2. Specimen preparation

### II.2.1. Abrasive water jet machining

The CFRP surface preparation by texturing operations have been performed with the AWJ machine ‘Flow Mach 4c’ (Flow International Corporation), equipped with Hyplex pump and Paser 4 nozzle. The abrasive particles selected for the machining operations were garnet sand in size of 120 mesh supplied by Wuxi Ding Long Minerals Co. Ltd (China). The plate is fastened on a wooden platform attached to the machining table to counteract any motion due to water splash during the machining process. The texturing path was a raster scan pattern parallel to the weft direction (cf. Fig. 1) with a 60 mm extension on each side of the plateto avoid over erosion arising from changes in traverse speed occurring due to the jet direction changes. The specimens have then been cut with the same waterjet machine.

To investigate the influence of the texturing quality on the adhesive properties of the bonded assemblies, three surface qualities, hereafter named “good”, “medium” and “poor” qualities, have been

produced by selecting different levels of waterjet pressure (P), jet traverse speed (V), scan step (SS) and standoff distance (SoD). These variable parameters are gathered in Table 1. Set values that have been selected for other machining parameters and are summed up in Table 2. All the selected values of the set and variable parameters are based on previous work concerning AWJ milling of 3D woven composite [8,9,22]. The depth of removal has been kept below 100 µm following the recommendations of Safran Aircraft Engines (SAE) and from the conclusions of a previous work on AWJ texturing of 3D woven CFRP composite [22]. Indeed, it was found that no significant deviation in the mechanical behaviour of the textured specimens (tensile static and tension-tension fatigue properties) was recorded when this specific condition is respected.

The dimensions of the specimens are consistent with the standards provided by Safran Aircraft Engines (AECMA standard prEN 6033). The CFRP/CFRP assemblies are composed of two plates sized 150 x 25 mm².For each surface quality, five replicates have been prepared. Five additional assemblies with surface preparation done by sanding at SAE were produced to have reference values of adhesive properties of the bonded assemblies.

### II.2.2. Machined surfaces and defects characterization

After the texturing operations, the profiles and the topographies of the obtained surfaces have been acquired by focus variation technique using the optical profilometer Infinite Focus SL from Alicona with the parameters gathered in Table 3. For both substrates of each specimen, a representative area of 15 mm x 15 mm was scanned, which permitted the quantification of the AWJ textured surface quality. This surface is considered as representative of both the material (several weaving meshes included) and the texturing process (around 10 jet passes over the scanned surface). As the main damage's shape is craters, the surface texturing has been estimated using a parameter called "crater volume per unit area" (Cv), following the procedure developed by Hejjaji et al. [10,17,23] and successfully used in former studies comprising 3D CFRP [8,22].

Scanning electron microscope (SEM) was used to furtherly characterize the textured surfaces. SEM images obtained from secondary electron (SE) sensor at 1000x magnification level was used to identify

the nature and form of various defects for each surface quality at specific regions of the treated surfaces viz. at the fibre/matrix interface, within the fibre tows and in the resin rich areas.

In order to compare Cv parameter's ability to correlate with adhesive properties of bonded assemblies with the one of the commonly used surface quality indicators, Mean Arithmetic Roughness (Ra) has been measured, both along ($Ra_L$) and perpendicular ($Ra_T$) to the texturing direction, from the topographies acquired by an optical profilometer. Therefore, the $Ra_L$ measurement corresponds to the roughness along the weft direction of the composite (cf. Fig. 1). A cut-off length (sampling length) of 0.8 mm and a total measured length of 15 mm have been used. Each Ra value presented hereafter corresponds to the mean of 5 measurements made along the zone of interest, as described in Fig. 2. Finally, Arithmetical Mean Height Sa has been quantified from each topography using identical parameters than Ra.

## II.3. Adhesive bonding operations

After the surface preparation done either by AWJ machining or sanding process, the textured faces of the substrates were cleaned using isopropyl alcohol. AF191K adhesive film, manufactured by 3M, with thickness of 135 µm, was used to bond the 3D woven CFRP textured adherents and shims were used at each extremity and each side of the plates to maintain bondline thickness. The pre-crack is made by a PTFE film (Teflon insert) with a nominal thickness of 20 µm going 20 mm inside the specimens. The assemblies are then placed in a vacuum bag (0.5 bar) and cured in an autoclave at a pressure of 3 bars and at 150°C for 3 hours. The heating and cooling rates of the curing procedure are 2°C/min and 1°C/min respectively.

## II.4. Mechanical characterization and instrumentation

Double Cantilever Beam (DCB) tests were conducted to investigate the influence of the AWJ textured surface quality on the adhesive behaviour of 3D woven composite assemblies. The test method followed standards provided by Safran Aircraft Engines (AECMA standard prEN 6033). However, the thickness of the substrates is higher than the value recommended by the standard (4.7 mm against 1.5 mm). This is a deliberate choice linked to the weaving architecture of the composite material. The material being the property of SAE, all the mechanical properties will be presented without scale or standardized by the reference (i.e. sanded specimens) ones.

The DCB tests were performed on INSTRON 8561 servo-hydraulic load frame with a 10 kN load cell. The specimens were subjected to a load piloted by a rate of 10 mm/min until achieving a crack propagation of at least100 mm. One side of each CFRP/CFRP assembly was speckle painted to record the strain during the tests by Digital Image Correlation (DIC).Cameras with a resolution of 5M pixels were used to film the zone of interest at 5 fps permitting to obtain a spatial resolution around 30 µm (cf. Fig. 3). An additional camera was positioned in order to follow the crack throughout the test.

# III. Results and discussion

As a matter of confidentiality, all the results presented hereafter and concerning the mechanical behaviour of the specimens are normalized by the values of the reference specimens (i.e. sanded 3D woven CFRP).

## III.1. Material removal and surface quality

The first step of this study was the characterization of the specimens' surface quality consecutive to AWJ texturing, i.e. the analysis of the substrates before bonding. Table 4 gathers the values of the textured depth as well as the different surface quality features (viz. Ra, Sa and Cv)for each set of machining parameters. Each cell presents the mean value of surface quality of both substrates adhesively bonded together. The machined depth of all the specimens, whatever the texturing method and/or quality is below 100 µm as targeted. Moreover, and as expected, increase in all the surface quality features have been recorded from "good" to "poor" qualities. For example, an increase of 78% and 134% has been noted in $Ra_L$ and Cv respectively. However, the differences in Ra ($Ra_L$ or $Ra_T$) are smaller than Sa or Cv between "good" and "medium" (around 4% and 21% respectively). In addition, around 53% of difference in $Ra_L$ has been noticed between sanded and "good" quality AWJ textured specimens, against smaller differences in Sa or Cv (9% and 1% respectively). Similar observations are made for the roughness when the transverse direction (i.e. weft direction) is considered ($Ra_T$). These observations are in accordance with previous work which has shown that classical surface quality criteria such as Ra (though being widely used in the industrial context), are local measurements which are not suitable to accurately correlate the surface quality of heterogeneous materials such as 3D woven CFRP composites and their mechanical behaviour [22]. The topographies of the textured surfaces of specimens with the different machining qualities are subjected to DCB tests are shown in Fig. 4. It can be seen that sanded and "good" AWJ specimens present similar surface texture, both in terms of depths and topologies, highlighted by

close values of Cv (0.418 $mm^3/cm^2$ and 0.423 $mm^3/cm^2$respectively for the sanded and AWJ "good" quality specimens). This will be an interesting information for the rest of this study, especially when analysing the link between the surface quality and the mechanical properties of the textured bonded assemblies.

In order to further analyse the textured surfaces, SEM pictures of specific zones of the textured surfaces for each machining quality have been taken (cf. Fig. 5 to Fig. 8). For all the texturing qualities, cracked, broken and bare fibres have been observed. In addition, matrix erosion around the fibres was noticed on specimens whose texturing conditions are the less harsh viz. sanded (cf. Fig. 5) and AWJ "Good" quality (cf. Fig. 6) specimens. Moreover, micro craters (several tens of microns in diameter) were found within the fibre tows, mainly located at the interface with the resin for sanded (cf. Fig. 5) and AWJ "Good" quality (cf. Fig. 6) specimens but also present in the middle of the fibre tows for AWJ "Medium"(cf. Fig. 7) and "Poor" qualities (cf.Fig. 8) specimens. These micro-craters can be linked to the deeply textured zones (depths close to 50°µm) presented in Fig. 4. All these types of defects have already been noticed in a previous work on AWJ machining of 3D woven CFRP composite material [8].A focus on the resin rich regions of the surfaces shows the presence of flat zones whose dimensions go from 20 µm to more than 80 µm in diameter. This can be explained by the fact that the epoxy resin is a brittle material which break into chips. The SEM picture of the matrix in Fig. 6 tends to prove this hypothesis. Indeed, cracks are observed in the resin. Once these cracks spread by the effect of water and join, a chip is formed and the matrix peels off as the chip breaks.

Finally, the textured specimens have been characterized by the X-ray tomography technique and no cracks originating from the machined surfaces or the cut edges were found. These observations are in accordance with previous work [8,22].

## III.2. Mode I fracture behaviour of the adhesively bonded CFRP/CFRP joints

The envelope curves of load-cross head displacement curves recorded during DCB tests for the different texturing qualities of the substrates are presented in Fig. 9. It can be seen that they are all similar in terms of general shape: indeed, as the crosshead displacement increases, the assemblies are subjected to

a load of decreasing amplitude, until reaching an asymptote. Each drop of load corresponds to an abrupt propagation of the crack between the two substrates constitutive of the adhesive bonded assemblies. However, these envelopes can be divided into two groups depending on the amplitude of the loads: one including both “sanded” and AWJ “good” quality specimens, the other (higher in loads than the first) containing AWJ “medium” and “poor” qualities assemblies. From this basic analysis, the assemblies having their substrates prepared by AWJ with “medium” or “poor” quality are expected to have a better mechanical behaviour under mode I loading.

This expectation is met as seen from Fig. 10which presents the evolution of the mean value of the critical energy release rate in Mode I ($G_{Ic}$) with respect to the different texturing quality of the adhesively bonded assemblies. In the case of surface quality description via 2D indicators ($Ra_L$ in Fig. 10a and $Ra_T$ in Fig. 10b), there are two plateaux of $G_{Ic}$, one for $Ra_L < 4.5$ µm or $Ra_T < 4$ µm, the second one 25% higher than the first for Ra values for $Ra_L > 4.5$ µm or $Ra_T > 4$ µm. When describing the surface quality by 3D indicators (such as Sa in Fig. 10c or Cv in Fig. 10d), the high plateau can still be observed, but both “sanded” and “AWJ good” cases are merged. This shows that there is a clearer link between the surface texturing quality of substrate surfaces described by 3D indicators and the mechanical behaviour of the bonded assemblies. This observation is in accordance with previous studies analysing the link between the textured surface quality and the static and fatigue mechanical behaviour of 3D woven CFRP [22] or CFRP laminates made of unidirectional plies [23,24]. However, given the high standard deviation of $G_{Ic}$, especially for “poor” AWJ texture quality specimens, it is interesting to analyse its evolution for each specimens individually to better understand the relationship between the surface quality and the critical energy release rate in mode I $G_{Ic}$. The 3D surface quality indicators being more appropriate to describe the textured surfaces of the assemblies, a focus is made on Sa and Cv.

The evolution of the critical energy release rate in Mode I with respect to the surface quality of the substrates defined by Sa (a) and Cv (b) is presented in Fig. 11 . All the $G_{Ic}$ values are standardized by the lowest critical energy release rate. When considering Sa as the indicator of textured surface quality, no additional information can be extracted concerning the relationship between $G_{Ic}$ and Sa. Indeed, despite the significant difference in critical energy release rate for the highest and lowest values for “poor” AWJ textured specimens (30%), there is no difference in Sa (around 1%). However, if the surface quality of the

substrates is quantified by the crater volume criterion Cv, a clear parabolic relationship ($R^2$=0.9302, against 0.6981 with Sa) can be found between the crater volume generated on 3D woven CFRP by AWJ texturing and the critical energy release rate in Mode I of CFRP/CFRP bonded assemblies. Indeed, an increase of 49% in critical energy release rate has been registered between assemblies with a crater volume of 0.40 and 0.58 $mm^3/cm^2$ respectively. However, as the crater volume still increases, the positive effect of AWJ texturing is less noticeable, with an increase of only 30% compared to the smallest value when Cv is 1.02 $mm^3/cm^2$. This means that there exists an optimum surface quality, comprised between 0.60 and 0.90 $mm^3/cm^2$, permitting to obtain the maximum critical energy release rate in Mode I, which exact amplitude cannot be estimated with the currently available data, more than 50% higher than the one obtained with the sanded specimens.

To explain this trend, the assembled specimens have been subjected to X-Ray tomography. The void percentage inside the adhesive layer of the bonded assemblies with respect to the crater volume of their substrates is presented in Fig. 12. It is seen that, as the crater volume increases, the void percentage drastically decreases: when Cv goes from 0.4 to 1.0 $mm^3/cm^2$, the void percentage drops from around 32% to 5%. For a better understanding of the phenomenon, mixed views (tomography and 3D topography) of the “good” and “poor” quality specimens are presented. In case of the “good” texturing quality, the voids (black dots on mixed views) are numerous and distributed through the surface, with no distinction of its topography. On the contrary, in case of the “poor” texturing quality, the voids are scarcer and mainly located in the craters created by the texturing process. Three assumptions are proposed for this change in void distribution. In the case where the “peaks” (resin rich areas between the fibre tows) of the textured surface of each substrate overlap when bonded, the adhesive might be expelled and trapped in the “valleys” – i.e. the craters corresponding to the location of the fibre tows (cf. Fig. 13a). A higher thermal conductivity of the bare carbon fibres compared to the epoxy matrix may promote the transition of the adhesive to the liquid state, favouring its flow and hence reducing the number of voids. In addition, the bare fibres might ease the displacement of the voids to the deepest zones of the textured substrates (i.e. the craters).Finally, small but deep craters on the textured surfaces, as observed on the SEM images (cf. Fig. 5 to Fig. 8), might not be filled by the adhesive due to its viscosity (cf. Fig. 13b).

The quantity of voids within the adhesive layer can be linked to the damage scenario of the specimens. Though all specimens fail cohesively, the fracture surfaces are different from one texturing quality to another. Indeed, ripped tows are found on assemblies whose substrates have been textured by AWJ with "poor" quality. To furtherly investigate this observation, an assembly of each texturing quality has been subjected to X-Ray tomography to follow the crack propagation path. It is clearly seen from Fig. 14 that the texturing quality of the substrates, hence the void volume inside the adhesive layer, influences the propagation of the crack. In the case of high void percentage, corresponding to sanded and AWJ "good" quality assemblies, the crack is quasi-straight and links the voids in the adhesive layer (pointed by arrows in Fig. 14). As the voids are less numerous (AWJ "Medium" and "Poor" qualities specimens), the crack's path becomes rugged and gets around the fibre tows, where the cohesion between the fibres and the matrix may be weaker than that between the tows and the adhesive due to the surface preparation. This assumption is supported by the topologies of the adherends in Fig. 4. The adhesive is directly in contact with the tows in the case of AWJ "poor" quality textured surfaces, making a bond between the adhesive and the fibre yarns even stronger that few voids are observed by X-Ray tomography. In the case of sanded or AWJ textured specimens with "good" quality, the adhesive is partially bonded to the matrix remaining on the fibre tows (cf. eroded matrix zones in Fig. 5 and Fig. 6) and the numerous voids within the adhesive layer make a weaker bond between the adhesive and the yarns. Secondary cracks and yarn bridging are also present on all the specimens. These different types of fracture mechanisms are in accordance with the literature treating crack propagation in mode I on 3D woven composites [18,19].

The transverse strain ($\varepsilon_{yy}$) maps of "sanded" and AWJ "medium" quality assemblies presented in Fig. 15 highlight these two crack propagation paths. Indeed, a clear circular zone of high strain permits to easily locate the crack tip of the "sanded" assembly and follow its propagation (cf. Fig. 15a). On the contrary, in the case of the AWJ "medium" quality assembly (cf. Fig. 15b), the zone of high strain is wider and deflected towards the fibre tows the closest to the crack tip. In both cases, the semi-circular zones of high strain from either side of the crack emphasize the presence of the secondary cracks around the fibres tows, which have already been noticed in the X-ray tomography pictures in Fig. 14.

The shear strain maps ($\varepsilon_{xy}$) obtained by DIC at a similar cross head displacement of 35 mm presented in Fig. 16 also confirm this hypothesis. High shear strains are recorded around the fibre tows along the

crack path for sanded and AWJ "good" quality assemblies, showing that the stress was not sufficient to rip off the tows. The crack hence follows the adhesive layer. As Cv increases, reduced zones of high strains are observed. This is originating from stress relief following the crack propagation around the tows.

# IV. Conclusion

The aim of this work was to study the influence of surface texturing of 3D interlock woven CFRP by AWJ machining process on the adhesive properties of 3D woven CFRP assemblies via DCB tests. Based on the findings presented in this paper, the following critical observations can be drawn:

- A parabolic relationship seems to exist between the crater volume generated on 3D woven CFRP by AWJ texturing and the critical energy release rate of CFRP/CFRP bonded assemblies. Indeed, an increase of 49% in the critical energy release rate has been registered between assemblies with a crater volume of 0.40 and 0.58 mm3/cm² respectively. However, as the crater volume increases, the positive effect of AWJ texturing is less noticeable, with an increase of only 30% compared to the smallest value when Cv is 0.99 mm3/cm². This means that there exists an optimum surface quality, comprised between 0.60 and 0.90 $mm^3/cm^2$, permitting to obtain the maximum critical energy release rate. Additional tests with adherends having a crater volume around this optimum value must be performed in order to validate this hypothesis. Moreover, a relationship between the viscosity of the adhesive and the crater volume must be investigated in the future.
- The crack propagation scenario is also linked to the surface quality of the adherend. Indeed, the crack path is straight through the adhesive bondline in case of adherend for low Cv (i.e. high void percentage in the adhesive layer), with few secondary crack formation and deflection. On the contrary, the crack path becomes rugged for high Cv (i.e. low void percentage), going around the fibre tows from one adherend to another in a sinusoidal way. This change can be related to the texturing process which removes the matrix on the fibre tows when machining is performed with harsher conditions, enhancing their bond with the adhesive. To furtherly characterize the adhesive bond between AWJ textured 3D woven CFRP specimens, single lap shear and three-point bending tests might be considered for understanding mode II and mixed mode behaviour.

**Acknowledgments**
The collaboration with Safran Aircraft Engines is gratefully acknowledged.

**References**


[1] Haddad M, Zitoune R, Eyma F, Castanié B. Study of the surface defects and dust generated during trimming of CFRP: Influence of tool geometry, machining parameters and cutting speed range. Compos Part A Appl Sci Manuf 2014;66:142–54.

[2] Nguyen-Dinh N, Zitoune R, Bouvet C, Le Roux S. Surface integrity while trimming of composite structures: X-ray tomography analysis. Compos Struct 2019;210:735–46.

[3] Haddad M, Zitoune R, Eyma F, Castanié B. Influence of Machining Process and Machining Induced Surface Roughness on Mechanical Properties of Continuous Fiber Composites. Exp Mech 2014;55:519–28.

[4] Ramulu M, Kramlich J. Machining of fiber reinforced composites: Review of environmental and health effects. Int J Environ Conscious Des Manuf 2004;11:1–19.

[5] Nguyen-Dinh N, Hejjaji A, Zitoune R, Bouvet C, Salem M. New tool for reduction of harmful particulate dispersion and to improve machining quality when trimming carbon/epoxy composites. Compos Part A Appl Sci Manuf 2020;131.

[6] Hashish M. An Investigation of Milling With Abrasive-Waterjets. J Eng Ind 1989;111:158.

[7] Ramulu M, Kunaporn S, Arola D, Hashish M, Hopkins J. Waterjet Machining and Peening of Metals. Analyzer 2000;122:90–5.

[8] Sourd X, Zitoune R, Hejjaji A, Salem M, Crouzeix L, Lamouche D. Multi-scale analysis of the generated damage when machining pockets of 3D woven composite for repair applications using abrasive water jet process: Contamination analysis. Compos Part A Appl Sci Manuf 2020;139:106118.

[9] Sourd X, Zitoune R, Crouzeix L, Salem M, Charlas M. New model for the prediction of the machining depth during milling of 3D woven composite using abrasive waterjet process. Compos Struct 2020;234.

[10] Hejjaji A, Zitoune R, Crouzeix L, Le Roux S, Collombet F. Surface and machining induced damage characterization of abrasive water jet milled carbon/epoxy composite specimens and their impact on tensile behavior. Wear 2017;376–377:1356–64.

[11] Cénac F, Zitoune R, Collombet F, Deleris M. Abrasive water-jet milling of aeronautic aluminum 2024-T3. Proc Inst Mech Eng Part L J Mater Des Appl 2013.

[12] Kumaran ST, Ko TJ, Uthayakumar M, Islam MM. Prediction of surface roughness in abrasive water jet machining of CFRP composites using regression analysis. J Alloys Compd 2017;724:1037–45.

[13] Kumaran ST, Ko TJ, Kurniawan R, Li C, Uthayakumar M. ANFIS modeling of surface roughness in abrasive waterjet machining of carbon fiber reinforced plastics. J Mech Sci Technol 2017;31:3949–54.

[14] Wingfield JRJ. Treatment of composite surfaces for adhesive bonding. Int J Adhes Adhes 1993;13:151–6.

[15] Baldan A. Adhesively-bonded joints and repairs in metallic alloys, polymers and composite materials: Adhesives, adhesion theories and surface pretreatment. J Mater Sci 2004;39:1–49.

[16] Zhang S, Panat R, Hsia KJ. Influence of surface morphology on the adhesion strength of epoxy-aluminum interfaces. J Adhes Sci Technol 2003;17:1685–711.

[17] Hejjaji A. Abrasive waterjet milling of CFRP composites and its influence on the mechanical behavior and patch adhesion intended for repair application. Université Paul Sabatier (Toulouse - France), 2018.

[18] Siddique A, Sun B, Gu B. Structural influences of two-dimensional and three-dimensional carbon/epoxy composites on mode I fracture toughness behaviors with rate effects on damage evolution. J Ind Text 2018.

[19] Siddique A, Sun B, Gu B. Finite element modeling on fracture toughness of 3D angle-interlock woven carbon/epoxy composites at microstructure level. Mech Adv Mater Struct 2019.

[20] Fishpool DT, Rezai A, Baker D, Ogin SL, Smith PA. Interlaminar toughness characterisation of 3D woven carbon fibre composites. Plast Rubber Compos 2013;42:108–14.

[21] Guénon VA, Chou TW, Gillespie JW. Toughness properties of a three-dimensional carbon-epoxy composite. J Mater Sci 1989;24:4168–75.

[22] Sourd X, Zitoune R, Crouzeix L, Coulaud M, Lamouche D. Influence of the damage generated by

abrasive water jet texturing on the tensile static and fatigue behaviour of 3D woven composite in the context of repair. Compos Part A Appl Sci Manuf 2021;149:106567.

[23] Hejjaji A, Zitoune R, Toubal L, Crouzeix L, Collombet F. Influence of controlled depth abrasive water jet milling on the fatigue behavior of carbon/epoxy composites. Compos Part A Appl Sci Manuf 2019;121:397–410.

[24] Nguyen-Dinh N, Bouvet C, Zitoune R. Influence of machining damage generated during trimming of CFRP composite on the compressive strength. J Compos Mater 2019.

**Fig. 1** Schematic view of the texturing path strategy.

**Fig. 2** Zones of measurements for Ra on the topologies of machined surfaces (15 x 15 mm) both parallel ($L_1$ to $L_5$) and perpendicular ($T_1$ to $T_5$) to the texturing direction.

**Fig. 3** Experimental setup used for Double Cantilever Beam tests.

**Fig. 4** Topographies of the substrates used for DCB tests after texturing with different machining qualities ($15 \times 15$ mm$^2$).

**Fig. 5** Optical cartography (top right) of a sanded specimen and SEM zoomed images of fibre (top left), interface (bottom left) and matrix (bottom right) areas.

**Fig. 6** Optical cartography (top right) of an AWJ "Good" quality specimen and SEM zoomed images of fibre (top left), interface (bottom left) and matrix (bottom right) areas.

**Fig. 7** Optical cartography (top right picture) of an AWJ "Medium" quality specimen and SEM zoomed images of matrix(top left), fibre (bottom left) and interface (bottom right) areas.

**Fig. 8** Optical cartography (top right picture) of an AWJ "Poor" quality specimen and SEM zoomed images of interface(top left), matrix (bottom left)and fibre (bottom right) areas.

**Fig. 9** Envelope of load-cross head displacement curves recorded during DCB tests for each texturing quality of the substrates.

**Fig. 10**Evolution of the critical energy release rate Mode I in function of the texturing processes as well as the surface quality indicators: (a) longitudinal $Ra_L$ and (b) transverse $Ra_T$ Mean Arithmetic Roughnesses, (c) surface Arithmetical Mean Height Sa and (d) crater volume Cv.

**Fig. 11** Evolution of the critical energy release rate in Mode I for the different machining qualities defined by: (a) surface roughness Sa and (b) crater volume Cv.

**Fig. 12** Evolution of the void percentage in the adhesive layer with respect to the crater volume and mixed view (tomography and 3D topography) of AWJ "good" and "poor" quality specimens.

**Fig. 13** Two possible scenarii explaining the presence of voids within the adhesive layer with (a) overlapping "peaks" expelling the voids in the "valleys" and (b) deep craters not filled with adhesive.

**Fig. 14** X-Ray tomography pictures of the specimen's crack tip at mid-width of the assemblies for each texturing quality. The arrows point to the voids in the adhesive layer.

**Fig. 15** Transverse strain maps showing the strain propagation path via two consecutive pictures for two texturing qualities: "sanded" and AWJ "medium". The arrows point to the crack tips.

**Fig. 16** Shear strain maps for a cross head displacement of 35 mm for the different texturing qualities.

**Table 1** Variable parameters selected for the texturing operations to generate several surface qualities.

| Parameter | Value | | |
|---|---|---|---|
| | Good | Medium | Poor |
| Pressure P (MPa) | 35 | 35 | 45 |
| Traverse speed V (m/min) | 16 | 14 | 14 |
| Scan step SS (mm) | 1.75 | 1.75 | 1.5 |
| Standoff distance SoD (mm) | 150 | 100 | 100 |

**Table 2** Set parameters selected for all the texturing operations.

| Parameter | Value |
|---|---|
| Focusing tube diameter | 1.016 mm |
| Focusing tube length | 76 mm |
| Nozzle diameter | 0.3302 mm |
| Type of abrasive | Garnet sand |
| Abrasive size | #120 |
| Abrasive flow rate | 0.18 kg/min |

**Table 3** Parameters selected for the profiles and topographies acquisition.

| Parameter | Value |
|---|---|
| Objective | 10x |
| Vertical resolution (µm) | 0.4 |
| Lateral resolution (µm) | < 8 |

**Table 4** Mean values of depth of removal (H), longitudinal and transverse surface roughness ($Ra_L$ and $Ra_T$), 3D surface roughness (Sa) and crater volume (Cv) and of the different specimens consecutive to AWJ texturing.

| Quality | H (µm) | $Ra_L$ (µm) | $Ra_T$ (µm) | Sa (µm) | Cv ($mm^3/cm^2$) |
|---|---|---|---|---|---|
| Sanded | 43.3 ± 17.5 | 2.788 ± 0.132 | 2.827 ± 0.170 | 7.967 ± 0.154 | 0.418 ± 0.011 |
| AWJ Good | 40.7 ± 18.6 | 4.271 ± 0.102 | 3.607 ± 0.053 | 8.670 ± 0.313 | 0.423 ± 0.018 |
| AWJ Medium | 48.0 ± 15.4 | 4.913 ± 0.038 | 4.294 ± 0.170 | 10.856 ± 0.184 | 0.561 ± 0.022 |
| AWJ Poor | 76.7 ± 17.1 | 7.611 ± 0.069 | 6.014 ± 0.143 | 19.847 ± 0.334 | 0.993 ± 0.039 |

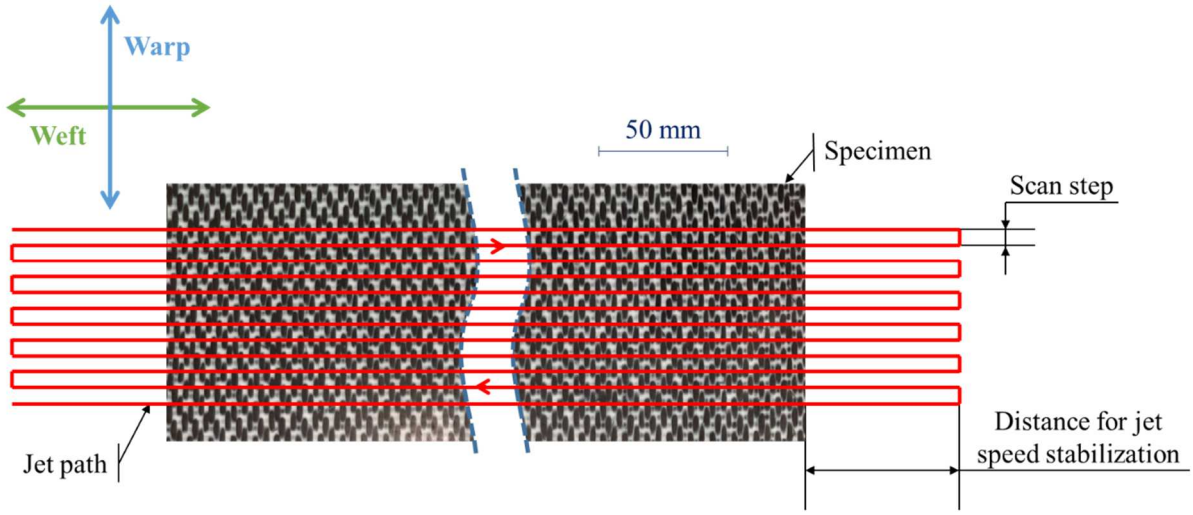


**Fig. 1** Schematic view of the texturing path strategy.

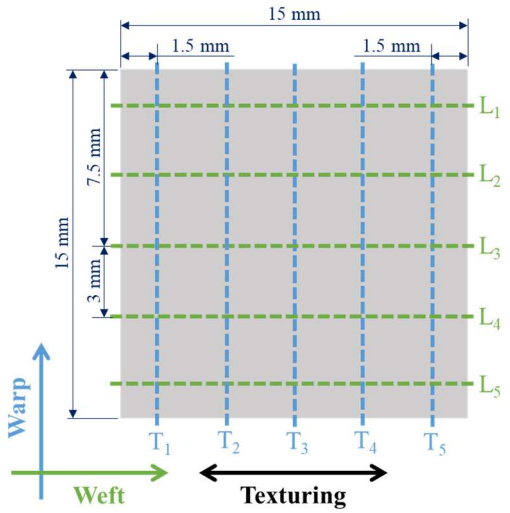


**Fig. 2** Zones of measurements for Ra on the topologies of machined surfaces (15 x 15 mm) both parallel ($L_1$ to $L_5$) and perpendicular ($T_1$ to $T_5$) to the texturing direction.

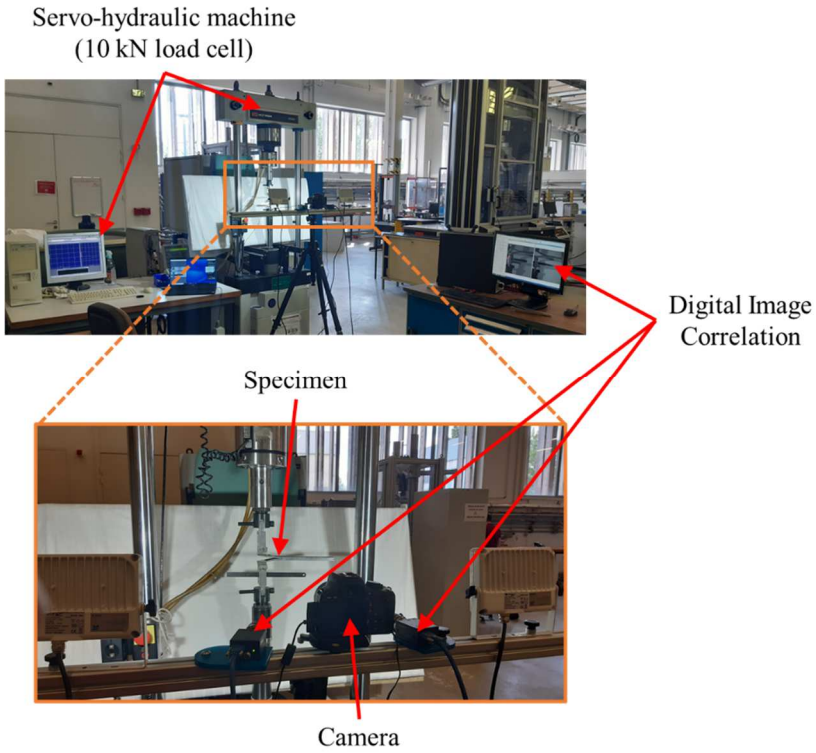


**Fig. 3** Experimental setup used for Double Cantilever Beam tests.

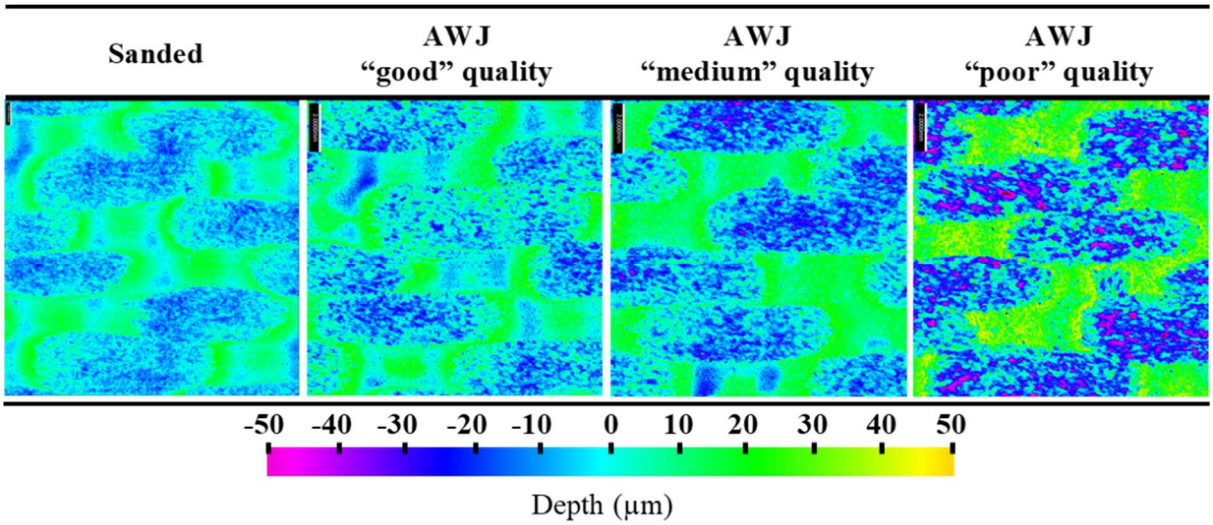


**Fig. 4** Topographies of the substrates used for DCB tests after texturing with different machining qualities ($15 \times 15$ mm$^2$).

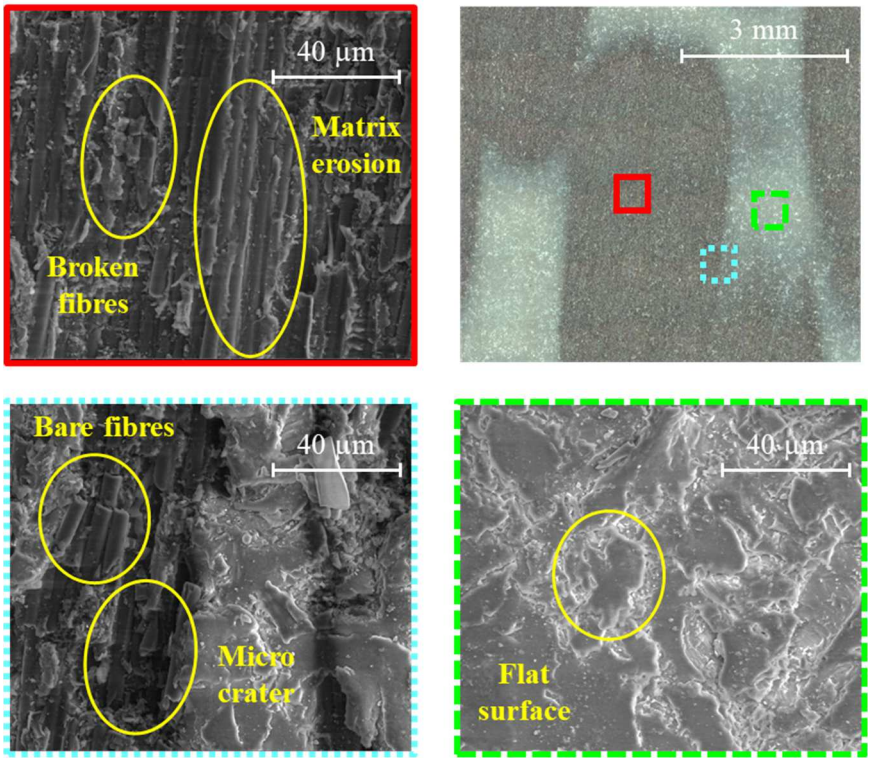


**Fig. 5** Optical cartography (top right) of a sanded specimen and SEM zoomed images of fibre (top left), interface (bottom left) and matrix (bottom right) areas.

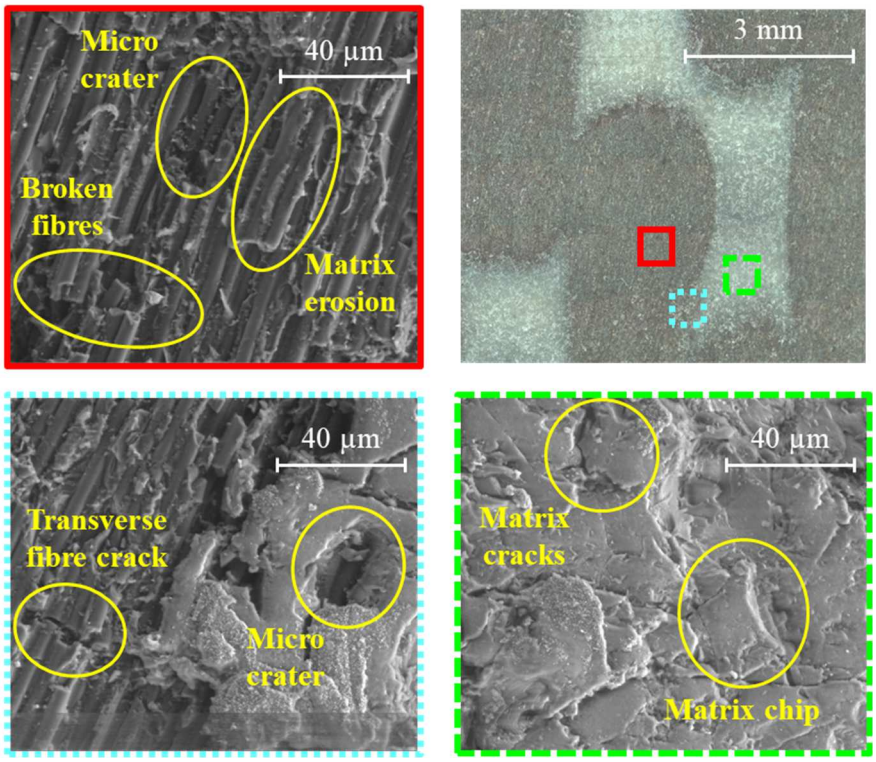


**Fig. 6**Optical cartography (top right) of an AWJ "Good" quality specimen and SEM zoomed images of fibre (top left), interface (bottom left) and matrix (bottom right) areas.

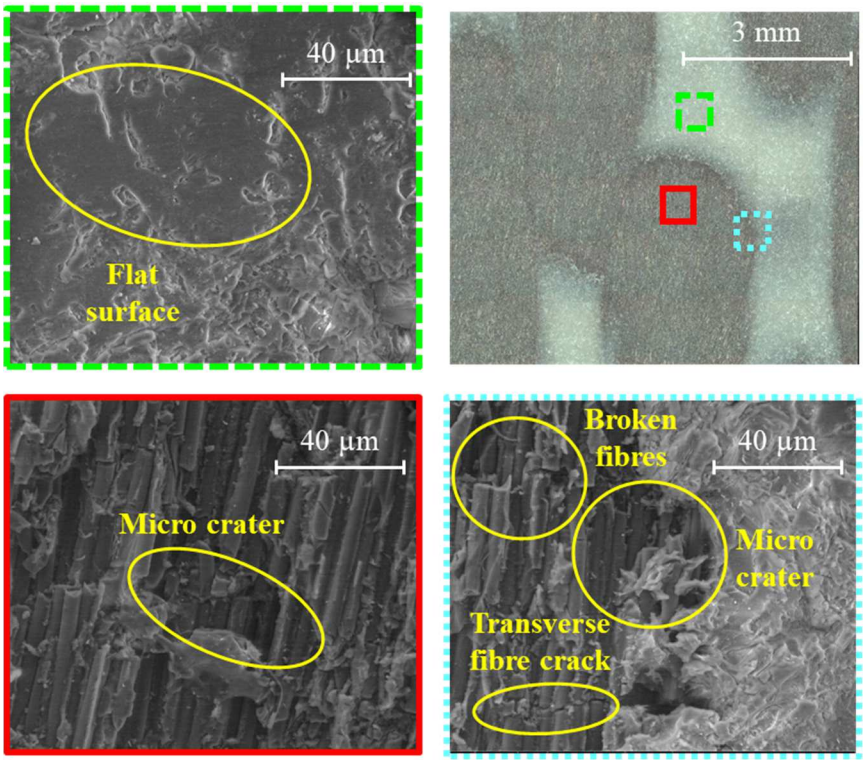


**Fig. 7**Optical cartography (top right picture) of an AWJ "Medium" quality specimen and SEM zoomed images of matrix(top left), fibre (bottom left) and interface (bottom right) areas.

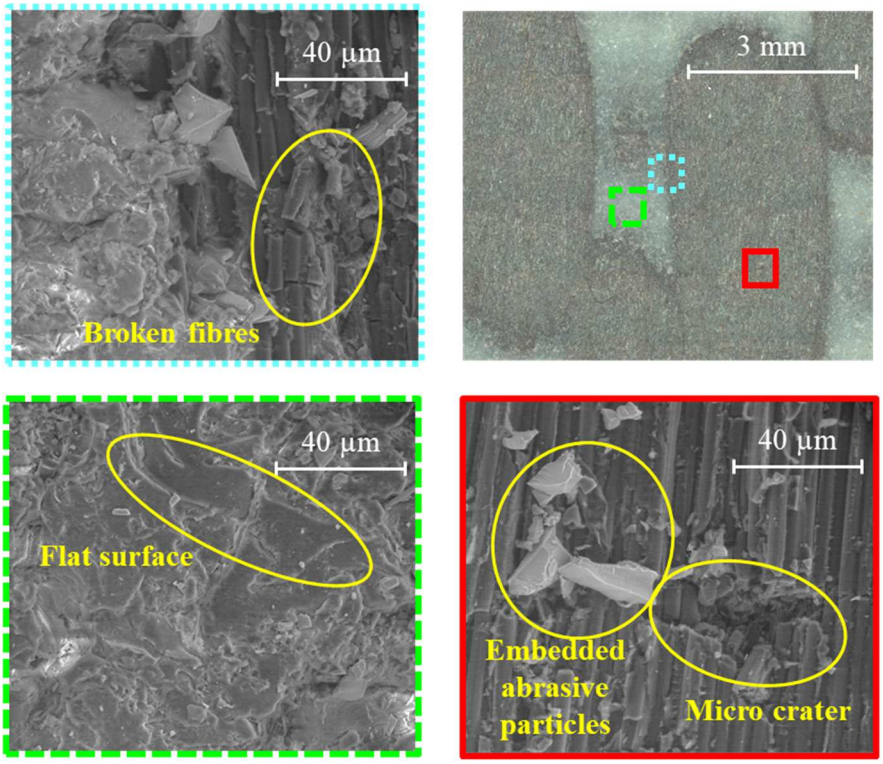


**Fig. 8**Optical cartography (top right picture) of an AWJ "Poor" quality specimen and SEM zoomed images of interface(top left), matrix (bottom left)and fibre (bottom right) areas.

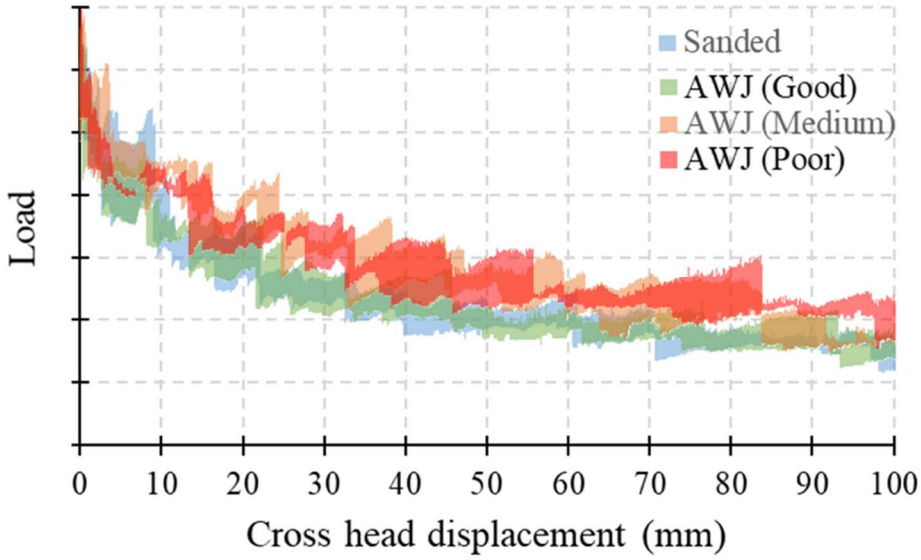


**Fig. 9** Envelope of load-cross head displacement curves recorded during DCB tests for each texturing quality of the substrates.

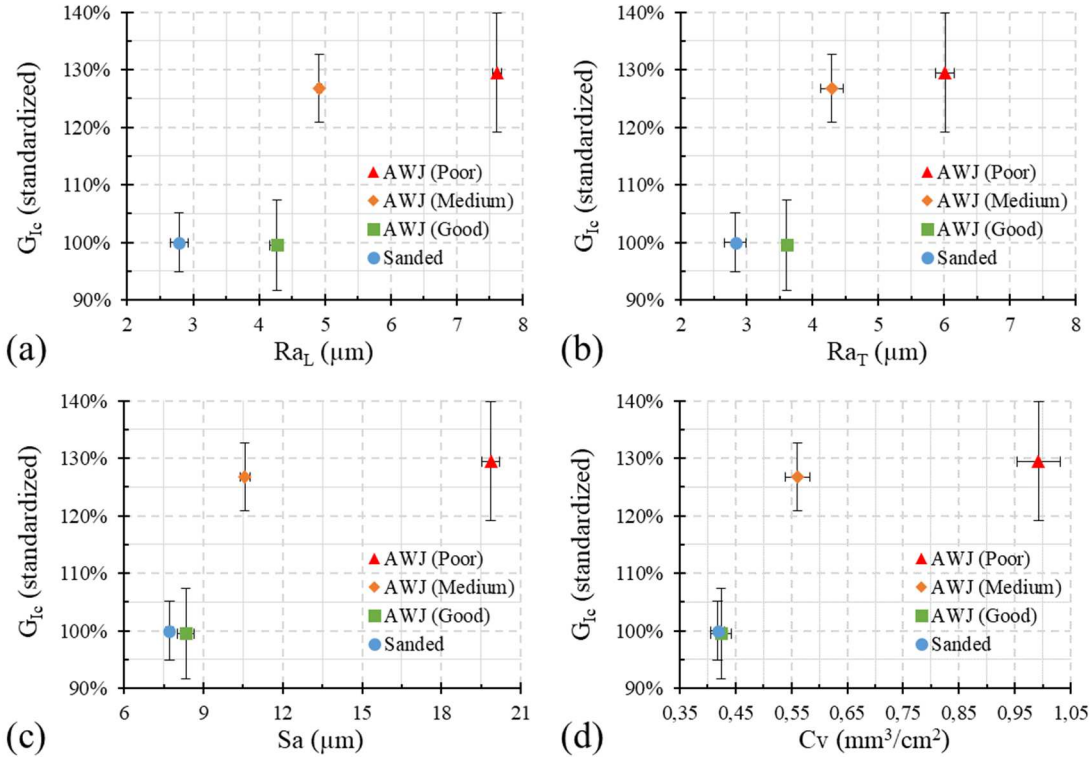


**Fig. 10**Evolution of the critical energy release rate Mode I in function of the texturing processes as well as the surface quality indicators: (a) longitudinal $Ra_L$ and (b) transverse $Ra_T$ Mean Arithmetic Roughnesses, (c) surface Arithmetical Mean Height Sa and (d) crater volume Cv.

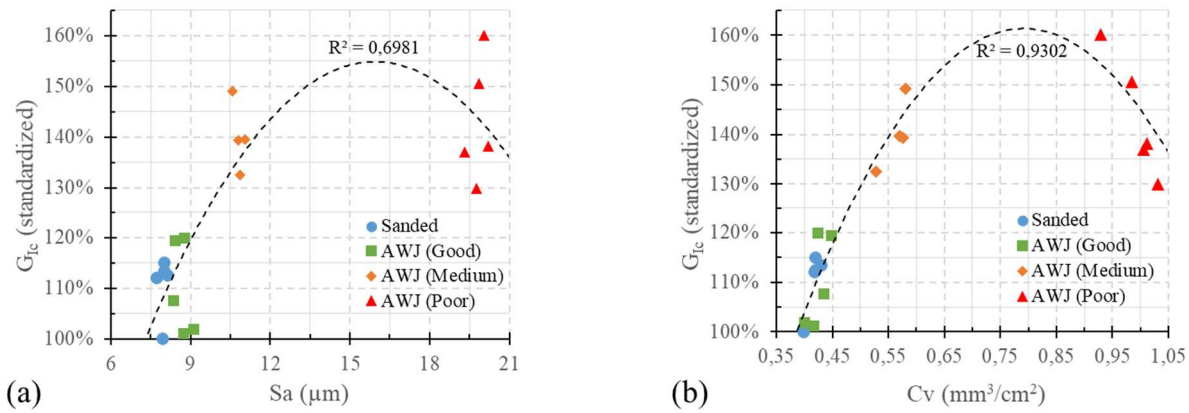


**Fig. 11** Evolution of the critical energy release rate in Mode I for the different machining qualities defined by: (a) surface roughness Sa and (b) crater volume Cv.

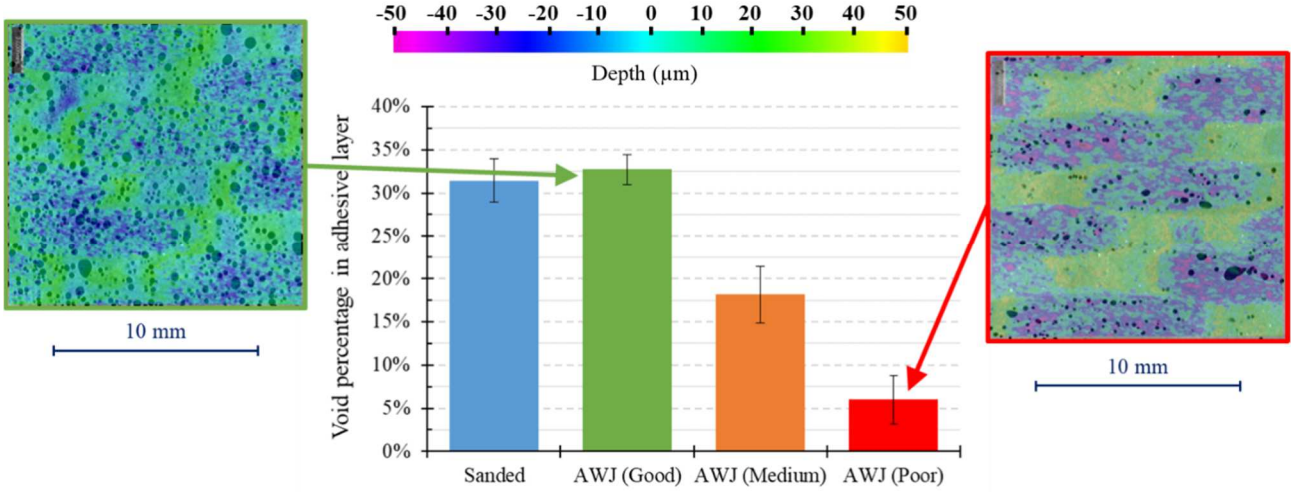


**Fig. 12** Evolution of the void percentage in the adhesive layer with respect to the crater volume and mixed view (tomography and 3D topography) of AWJ "good" and "poor" quality specimens.

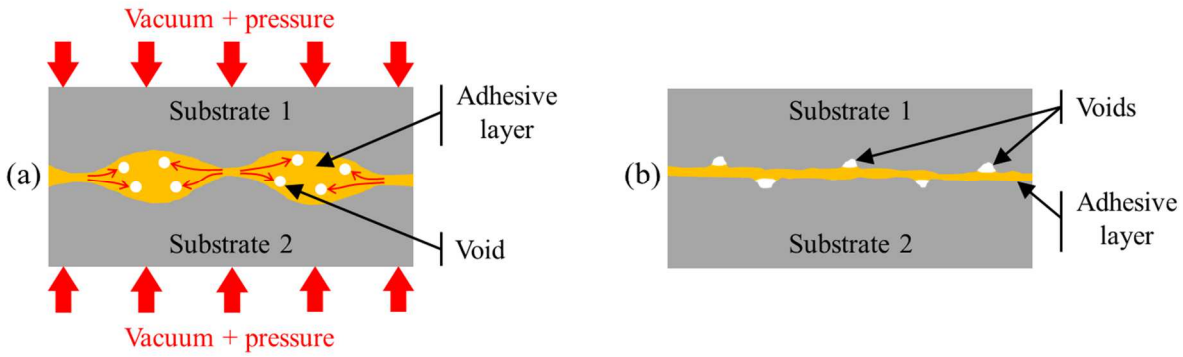


**Fig. 13** Two possible scenarii explaining the presence of voids within the adhesive layer with (a) overlapping "peaks" expelling the voids in the "valleys" and (b) deep craters not filled with adhesive.

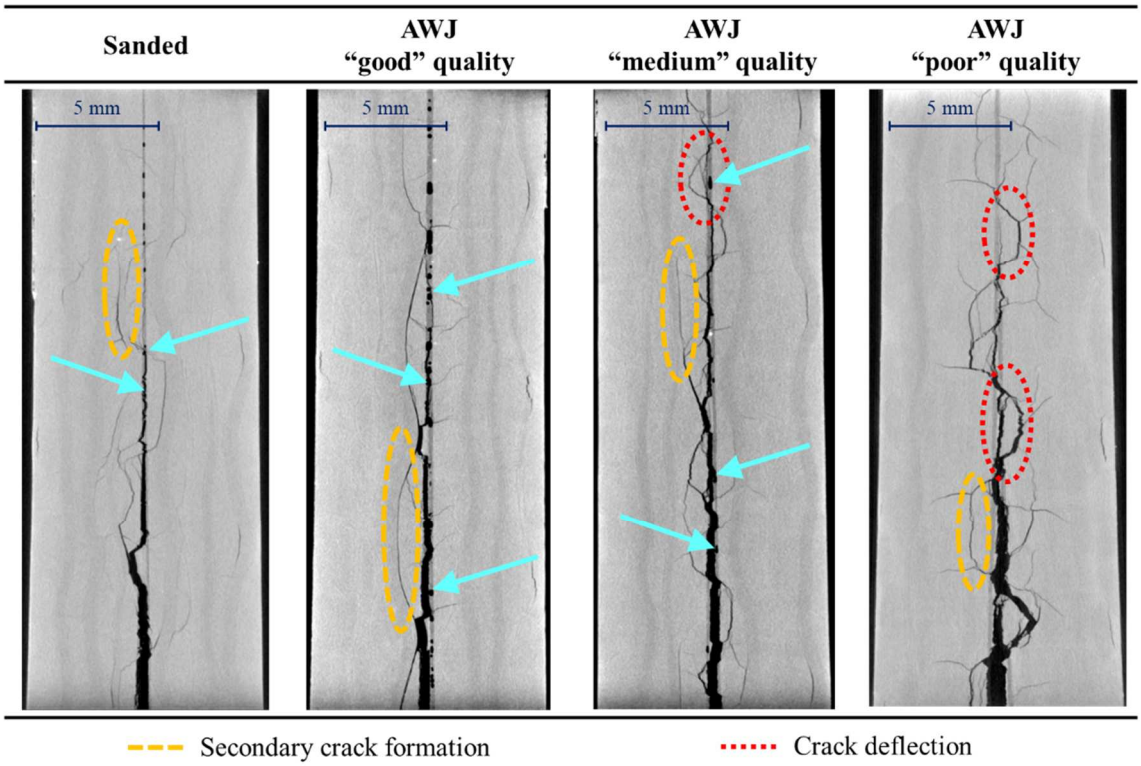


**Fig. 14** X-Ray tomographic images of the specimen's crack tip at mid-width of the assemblies for each texturing quality. The arrows point to the voids in the adhesive layer.

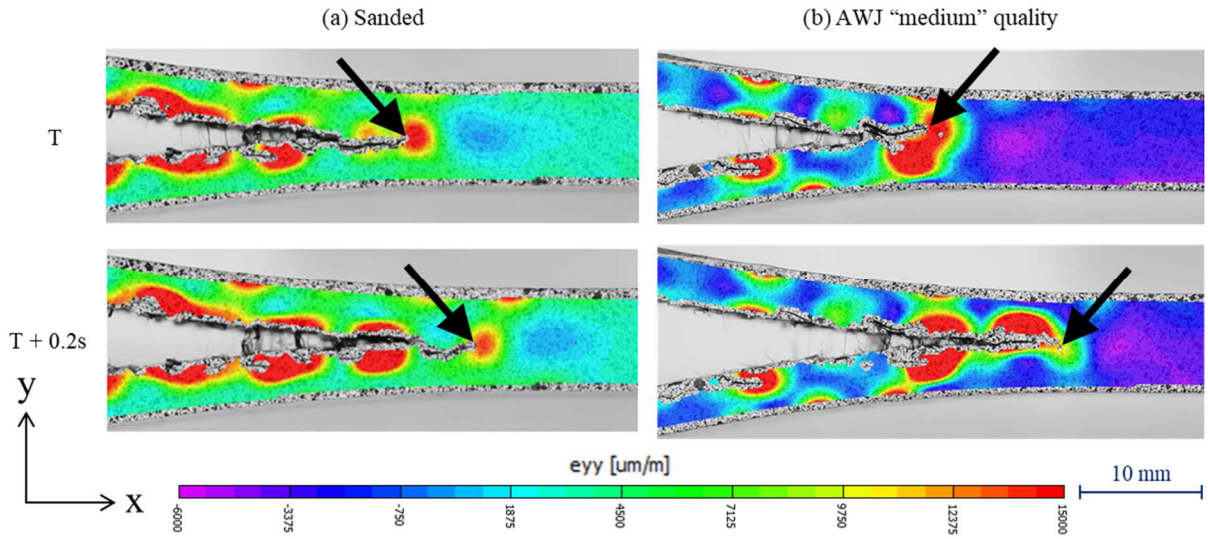


**Fig. 15** Transverse strain maps showing the strain propagation path via two consecutive pictures for two texturing qualities: "sanded" and AWJ "medium". The arrows point to the crack tips.

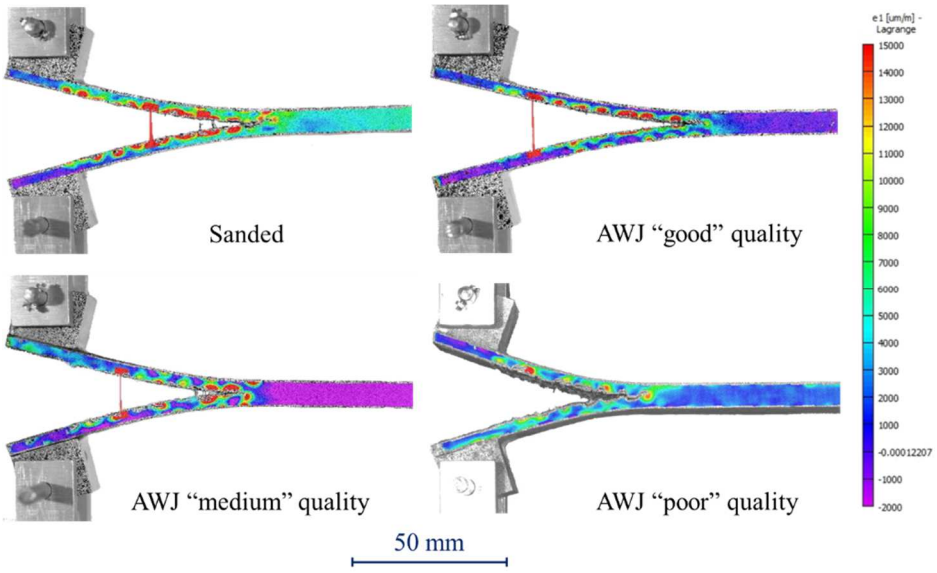


**Fig. 16** Shear strain maps for a cross head displacement of 35 mm for the different texturing qualities.